# A conservative finite difference scheme for Poisson–Nernst–Planck equations

**Allen Flavell · Michael Machen · Bob Eisenberg ·
Julienne Kabre · Chun Liu · Xiaofan Li**

**Abstract** A macroscopic model to describe the dynamics of ion transport in ion channels is the Poisson–Nernst–Planck (PNP) equations. In this paper, we develop a finite-difference method for solving PNP equations, second-order accurate in both space and time. We use the physical parameters specifically suited toward the modeling of ion channels. We present a simple iterative scheme to solve the system of nonlinear equations resulting from discretizing the equations implicitly in time, which is demonstrated to converge in a few iterations. We place emphasis on ensuring numerical methods to have the same physical properties that the PNP equations themselves also possess, namely conservation of total ions, correct rates of energy dissipation, and positivity of the ion concentrations. We describe in detail an approach to derive a finite-difference method that preserves the total concentration of ions exactly in time. In addition, we find a set of sufficient conditions on the step sizes of the numerical method that assure positivity of the ion concentrations. Further, we illustrate that, using realistic values of the physical parameters, the conservation property is critical in obtaining correct numerical solutions over long time scales.

A. Flavell · M. Machen · J. Kabre · X. Li (✉)
Department of Applied Mathematics, Illinois Institute
of Technology, 10 W. 32 St., Chicago, IL 60616, USA
e-mail: lix@iit.edu

*Present address:*
M. Machen
Department of Applied and Computational Mathematics
and Statistics, University of Notre Dame, 153 Hurley Hall,
Notre Dame, IN 46556, USA

B. Eisenberg
Department of Molecular Biophysics and Physiology,
Rush Medical Center, 1653 West Congress Parkway, Chicago,
IL 60612, USA

C. Liu
Department of Mathematics, Pennsylvania State University,
University Park, PA 16802, USA

## 1 Introduction

The Poisson–Nernst–Planck (PNP) equations describe the diffusion of ions under the effect of an electric field that is itself caused by those same ions. The system is created by coupling the Nernst–Planck equation (which describes the diffusion of ions under the effect of an electric potential) with the Poisson equation (which relates charge density with electric potential). This system of equations has found much use in the modeling of semiconductors [24]. Although the Poisson–Nernst–Planck equations were applied to model membrane transport for longer than they have been employed to model semiconductors [30], the use of the system to model the behavior of the internal mechanics of these transport processes is much more recent [8].

The system of PNP equations and its related models have been the subject of much study and numerical simulation. A recent advancement in this field was the application of energy variational analysis and density functional theory to modify the PNP system to accommodate various phenomena exhibited by biological ion channels. See [32] and the references therein.

The computer simulations of the Poisson–Nernst–Planck models are able to capture the transient, dynamical behavior of the system, and the numerical schemes employed are quite varied. Cagni *et al.* (2007) [3] discretized the PNP in

two dimensions using a second-order accurate finite difference method with central differencing in space and Crank–Nicolson scheme in time, and simulated an ion channel subjected to time-dependent perturbations. Nanninga (2008) [27] studied a nerve impulse using a similar finite difference scheme as in [3] but in three dimensions, notable in that it directly included gating and selectivity into the model. Lopreore *et al.* (2008) [23] developed a finite-volume-based technique to solve PNP in three dimensions, which decomposes the domain using a dual Delaunay–Voronoi mesh. Neuen (2010) [28] developed a semi-implicit finite element-based scheme to simulate three-dimensional, multi-scale extended PNP. Gardner and Jones (2011) [10] simulated a potassium channel modelled with PNP in two dimensions using a finite difference method with TR-BDF2 time integration. Much of the numerical schemes in [10] is based on the previous work [11], a one-dimensional model of the same channel. Hyon *et al.* (2011) [19] presented another finite element method with back-Euler method in time to investigate the effects of finite size of the ions by modifying the PNP via introducing a repulsive potential energy into the total energy. Horng *et al.* (2012) [17] applied the multiblock Chebyshev pseudospectral method and the method of lines to solve a one-dimensional modified PNP modeling the finite-sizeness of the ions via a local model.

One of the characteristics of the nonlinear PNP equations is that its overall behavior is very sensitive to the boundary conditions [13]. This presents a challenge for accurate and efficient numerical simulations, as generally the boundary conditions will have to be discretized and approximated. In this paper, we shall investigate the effects of discretization error on the Poisson–Nernst–Planck equations, in particular discretization of the boundary conditions and the equations at the boundaries. We will demonstrate that the conservation properties of the numerical methods could be critical in obtaining the long-time behavior of the solutions.

To our knowledge, relatively few studies describe numerical methods such as finite difference method, finite element method, finite volume method and many others for solving partial differential equations (PDEs), which *preserve the physical quantities underlying the PDEs exactly at the discrete level*. Fisher *et al.* (2012) [9] developed finite difference methods for solving the Euler equations and the Burgers equation that relied on using specific split forms of the equations to preserve the discrete energy dynamics. Hof and Veldman (2012) [16] developed finite volume discretizations for the 1D and 2D Euler equations, as well as the 1D and 2D Shallow Water equations, which conserved the dynamics of mass, momentum and energy of the systems. For the incompressible Navier–Stokes equations, the papers [14, 15, 20, 25, 26, 31] presented finite difference discretizations on uniform or nonuniform grids that preserve part or all of discrete mass, momentum, and kinetic energy.

Li and Vu-Quoc (1995) [22] developed a finite difference method for solving the nonlinear Klein–Gordon equation which preserved the total discrete energy. Qiao *et al.* (2011) [29] showed unconditionally energy stable finite difference schemes for the dynamics of the molecular beam epitaxy, which preserves the energy decay rate exactly at the discrete level. Zhang and Qiao (2012) [33] proposed a finite difference scheme that is mass-conservative and preserves energy decay rate precisely for the Cahn–Hilliard equation. Celledoni *et al.* (2012) [4] developed a general method of discretizing partial differential equations that preserved the total energy exactly, based on the average vector field method. Chiu *et al.* (2012) [5] developed a general meshfree scheme for solving partial differential equations characterized by conservation of the discrete energy, and they demonstrated its effectiveness by solving the 1D and 2D inviscid advection equations.

It is also rare for numerical schemes to preserve positivity for nonlinear advection-diffusion equations like PNP, which do not have a maximum principle. The work on this topic is well summarized by Hundsdorfer and Verwer[18]. Bolley and Crouzeix [2] developed much of the theory, establishing that linear single-step and multi-step methods of second-order or higher in time cannot preserve positivity unconditionally, and obtaining necessary and sufficient conditions for positivity preservation for certain classes of numerical methods.

The paper is organized as follows. We start by defining and simplifying the equations we are working with, in Sect. 2, including the introduction of the quantities that shall be preserved by our numerical schemes: the total concentration of each ion species in Sect. 2.1 and the energy dissipation law in Sect. 2.2. We then describe our numerical schemes in Sect. 3, which presents an approach to conserve the total ion concentrations exactly, preserve positivity of the ion concentrations, and approximate the energy dissipation law closely. Finally, we shall discuss the results of simulating the system using our numerical schemes in Sect. 4.

## 2 Governing equations

Consider the PNP equations [8, 11]

$$\frac{\partial c_i}{\partial t} = \nabla \cdot \left\{ D_i \left[ \nabla c_i + \frac{z_i e}{k_B T} c_i \nabla \phi \right] \right\}, \tag{1}$$

$$i = 1, 2, \ldots, N,$$

$$\nabla \cdot (\epsilon \nabla \phi) = -\left( \rho_0 + \sum_{i=1}^{N} z_i e c_i \right), \tag{2}$$

where $c_i$ is the ion density for the $i$-th species, $D_i$ is the diffusion constant, $z_i$ is the valence, $e$ is the unit charge,

$k_B$ is the Boltzmann constant, $T$ is the absolute temperature, $\epsilon$ is the permittivity, $\phi$ is the electrostatic potential, $\rho_0$ is the permanent (fixed) charge density of the system, and $N$ is the number of ion species [19]. The equations are valid in a bounded domain $\Omega$ with boundary $\partial\Omega$ and for time $t \geq 0$.

In this work, we shall use the no-flux boundary condition for Eq. (1). This may correspond to modeling the interior conditions of a channel that is in an occluded state, with closed gates at either end. Simulations of channels such as the KirBac1.1 channel in such a state have been conducted in the past [6]. We shall use the Robin boundary condition for the Poisson equation, which models the effects of making the source of the potential across the channel partially removed from the ends of the channel. The formula for the boundary conditions are

$$D_i\left[\nabla c_i + \frac{z_i e}{k_B T}\nabla c_i \phi\right]\cdot \mathbf{n} = 0, \quad i = 1, 2, \ldots, N, \tag{3a}$$

$$(\phi - \phi_\pm) + \eta\frac{\partial\phi}{\partial\mathbf{n}} = 0, \tag{3b}$$

for points on the boundary $x \in \partial\Omega$.

For some situations, such as a generic potassium channel separating potassium and chloride ion baths, the experimental data can be well-approximated by a one-dimensional model [11]. In one dimension, Eqs. (1) and (2) are simplified as

$$\frac{\partial c_i}{\partial t} = \frac{\partial}{\partial x}\left[D_i\left(\frac{\partial c_i}{\partial x} + \frac{z_i e}{k_B T}c_i\frac{\partial\phi}{\partial x}\right)\right] \tag{4}$$

$$\frac{\partial}{\partial x}\left(\epsilon\frac{\partial\phi}{\partial x}\right) = -\left(\rho_0 + \sum_i z_i e c_i\right), \tag{5}$$

for $-L \leq x \leq L$ and $t \geq 0$, where $L$ is the half of the length of the ion channel. The corresponding boundary conditions are

$$D_i\left(\frac{\partial c_i}{\partial x} + \frac{z_i e}{k_B T}c_i\frac{\partial\phi}{\partial x}\right) = 0,$$
$$(\phi - \phi_\pm) \pm \eta\frac{\partial\phi}{\partial x} = 0, \quad \text{for } x = -L, L. \tag{6}$$

### 2.1 Total concentration

The total concentration per ion species is given by

$$c_{i,tot}(t) = \int_{-L}^{L} c_i(x, t)\,dx, \quad i = 1, 2, \ldots, N. \tag{7}$$

Due to the no-flux boundary conditions (6), the total concentration of each ion species is constant in time. This can be verified easily by differentiating (7) with respect to time, then applying the convection-diffusion equation (4) and no flux boundary condition (6).

One of the metrics we can use to evaluate different numerical schemes is therefore to measure how well the total concentration is conserved in numerical simulation. Ensuring that the total concentration for each species $c_{i,tot}$ is constant will be the idea behind the schemes presented in this work. As will be seen in Sect. 4, the preservation of the conservation property is crucial for producing correct numerical results over long time scales.

### 2.2 Energy dissipation

The governing equations (4) and (5) for the transport of ions can be derived from the energy of the system using variational principles. Similar to [19], the total energy for our specific system is defined by

$$E = \int_{-L}^{L}\left[k_B T\sum_{i=1}^{N} c_i\log\frac{c_i}{c_{i,0}} + \frac{1}{2}\left(\rho_0 + \sum_{i=1}^{N} z_i e c_i\right)\phi\right]dx$$
$$+ \frac{\epsilon}{2\eta}\left(\phi_+\phi(L) + \phi_-\phi(-L)\right), \tag{8}$$

where $c_{i,0}$ are constants called "reference concentrations". Using the Poisson equation (5), the total energy can be written as

$$E = \int_{-L}^{L}\left[k_B T\sum_{i=1}^{N} c_i\log\frac{c_i}{c_{i,0}} + \frac{\epsilon}{2}\left(\frac{\partial\phi}{\partial x}\right)^2\right]dx$$
$$+ \frac{\epsilon}{2\eta}\left(\phi^2(L) + \phi^2(-L)\right), \tag{9}$$

where the last term is the contribution of the electric energy from the boundaries. The total energy $E$ satisfies the energy dissipation property

$$\frac{dE}{dt} = -\int_{-L}^{L}\sum_{i=1}^{N}\frac{D_i}{k_B T}c_i\left|\frac{\partial\mu_i}{\partial x}\right|^2 dx, \tag{10}$$

where $\mu_i$ is the chemical potential of $i$'th ion species defined by the variational derivative of the energy with respect to the concentration $c_i$

$$\mu_i = \frac{\delta E}{\delta c_i} = k_B T\left(\log\frac{c_i}{c_{i,0}} + 1\right) + z_i e\phi. \tag{11}$$

The energy dissipation law (10) can be derived by taking the time derivative of the total energy (8) and applying integration by parts, Eqs. (4)–(5) and the boundary condition (6):

$$\frac{dE}{dt} = \int_{-L}^{L} k_B T\sum_i\left(\log\frac{c_i}{c_{i,0}} + 1\right)\frac{\partial c_i}{\partial t}\,dx$$
$$+ \int_{-L}^{L}\left[\frac{1}{2}\sum_i z_i e\frac{\partial c_i}{\partial t}\phi + \frac{1}{2}\left(\rho_0 + \sum_i z_i e c_i\right)\frac{\partial\phi}{\partial t}\right]dx$$

$$+ \frac{\partial}{\partial t}\left[ \frac{\epsilon}{2\eta}\big(\phi_+\phi(L) + \phi_-\phi(-L)\big)\right]$$

$$= -\int_{-L}^{L} \sum_i \frac{D_i}{k_B T} c_i \left|\frac{\partial \mu_i}{\partial x}\right|^2 \mathrm{d}x$$

$$- \frac{1}{2}\epsilon\left(\frac{\partial \phi}{\partial x}\frac{\partial \phi}{\partial t} - \frac{\partial^2 \phi}{\partial x \partial t}\phi\right)\Bigg|_{-L}^{L}$$

$$+ \frac{\partial}{\partial t}\left[ \frac{\epsilon}{2\eta}\big(\phi_+\phi(L) + \phi_-\phi(-L)\big)\right]. \tag{12}$$

The rate of energy decay (10) can be obtained by using the boundary condition (6) to show the last two terms on the RHS of (12) cancel each other.

## 2.3 Parameters and nondimensionalization

We specify the units and the parameters using the approximate values corresponding to the KcsA potassium channel [7]. In our 1D model, the cylindrical channel takes a diameter of 10 Å and a length of 120 Å. We shall assume no permanent charges or selectivity for the purposes of this simulation. We consider the case of two ion species, i.e. $N = 2$, with the initial concentration for each ion being 2 molar, resulting in an initial number density (number of ions per unit volume) of $1.2044 \times 10^{-3}$ ions/Å$^3$. The combination of the parameters $k_B T/e$ is approximately 0.025 V, assuming the temperature is $T = 298$ K. The permittivity $\epsilon = \epsilon_r \epsilon_0$ is determined by the value of the vacuum $\epsilon_0 = 8.854187817 \times 10^{-12}$ F/m and the relative permittivity $\epsilon_r$ (78.5 for water).

The values of the diffusion coefficients $D_i$ depend on both the ion species and the channel. The only net effect of different diffusion constants is the rate of evolution of the system. Typical values for the diffusion coefficients for ion species in a channel are around $10^9$ Å$^2$/s [12]. We will select both diffusion coefficients to be equal to each other, causing them to take a value of one after nondimensionalization.

The parameter $\eta$, as a component of the Robin boundary condition (3b), is an aggregate of multiple physical constants and is highly dependent on the properties of the surrounding membrane. modeling the experimental setup as an electrical circuit shows that the quantity $A\epsilon_l/\eta$, where $A$ is the area of the membrane and $\epsilon_l$ is the permittivity of the membrane, has units of capacitance and is related to charge storage. The most significant charge storage contributing to $A\epsilon_l/\eta$ is in fact the membrane capacitance, so we may surmise that the primary contributor to $\eta$ is the membrane capacitance. If a very high capacitance to ground is present, $\eta$ is approximated by the appealing formula $\eta = A\epsilon_l/C$, where $C$ is the capacitance of the membrane, however realistically $\eta$ is much smaller than that. In this work, we shall take $\eta = 2.78 \times 10^{-3}$ Å for our numerical simulations, but

will also examine the effects of $\eta$ over a range from $10^{-5}$ Å to 60 Å. Changing the value of $\eta$ might correspond to adding a parallel capacitance in experiment.

Define the dimensionless variables and parameters $c_i' = c_i/c_0$, $x' = x/L$, $t' = t/(L^2/D_0)$, $D_i' = D_i/D_0$, $\phi' = \phi/\phi_0$, and $\rho_0' = \rho_0/(ec_0)$ where $c_0$ is the average of the initial charge concentration, $L$ is the half of the channel length or computational domain, $D_0$ is a typical diffusion coefficient, $\phi_0$ is a characteristic value of the electrostatic potential such as the boundary value. Then, non-dimensionalizing the Nernst–Planck equation (4), we obtain

$$\frac{\partial c_i'}{\partial t'} = \frac{\partial}{\partial x'}\left\{ D_i'\left[ \frac{\partial c_i'}{\partial x'} + \chi_1\left(z_i c_i' \frac{\partial \phi'}{\partial x'}\right)\right]\right\}, \tag{13}$$

where $\chi_1 := e\phi_0/k_B T$. From the above, the dimensionless parameter $\chi_1 \approx 3.1$, if $\phi_0 = 0.08$ V. The nondimensionalized Poisson equation (5) is given by

$$\frac{\partial}{\partial x'}\left(\epsilon' \frac{\partial \phi'}{\partial x'}\right) = -\chi_2\left(\rho_0' + \sum_i z_i c_i'\right), \tag{14}$$

where $\chi_2 := \frac{ec_0 L^2}{\phi_0 \epsilon_t}$. Here, the dimensionless parameter $\epsilon'$ is defined as $\epsilon' := \epsilon/\epsilon_t$ where $\epsilon_t$ is the characteristic permittivity chosen to be the value for water: $\epsilon_t = 6.950537436 \times 10^{-20}$ F/Å. The non-dimensional parameter $\chi_2$ is approximately 125.4 with these values. The corresponding dimensionless boundary conditions are

$$D_i'\left[ \frac{\partial c_i'}{\partial x'} + \chi_1\left(z_i c_i' \frac{\partial \phi'}{\partial x'}\right)\right] = 0,$$
$$\big(\phi' - \phi_\pm'\big) + \eta' \frac{\partial \phi'}{\partial \mathbf{n}} = 0, \quad \text{for } x = -1, 1, \tag{15}$$

where $\eta' := \eta/L$.

We drop the primes when we present our numerical methods for clarity.

## 3 Numerical methods

We present a method for deriving numerical schemes that would conserve total concentration of each ion species exactly if computations were performed without round-off errors. We will illustrate the method by describing a mass-conservative scheme (i.e. preserving ion concentration exactly) for solving the nonlinear systems of PDEs (13) and (14). The extension of the method to the multidimensional case is straightforward. This scheme uses the trapezoidal rule and the second-order backward differentiation formula (TR-BDF2) in time and the second-order central differencing in space. The TR-BDF2 scheme is implicit in time, resulting in a system of nonlinear equations after discretization. Instead of using the Newton–Raphson

method for solving the large nonlinear systems at each time step, we present a simple iterative scheme which is easy to implement and can solve the systems efficiently.

### 3.1 Discretization in time

For time-stepping, we shall use a slight modification of the scheme described in [1], which combines the trapezoidal rule with the second-order backward differentiation formula.

(1) TR step:

$$c_i^{n+\gamma,k+1} - \gamma\frac{\Delta t_n}{2}f\left(c_i^{n+\gamma,k+1}, \phi^{n+\gamma,k}\right)$$
$$= c_i^n + \gamma\frac{\Delta t_n}{2}f\left(c_i^n, \phi^n\right), \quad i = 1, 2,$$
$$\frac{\partial}{\partial x}\left(\epsilon\frac{\partial\phi^{n+\gamma,k+1}}{\partial x}\right) = -\chi_2\left(\rho_0 + \sum_{i=1}^2 z_i c_i^{n+\gamma,k+1}\right), \tag{16}$$

for $k = 0, 1, 2, \ldots$.

(2) BDF2 step:

$$c_i^{n+1,l+1} - \frac{1-\gamma}{2-\gamma}\Delta t_n f\left(c_i^{n+1,l+1}, \phi^{n+1,l}\right)$$
$$= \frac{1}{\gamma(2-\gamma)}c_i^{n+\gamma} - \frac{(1-\gamma)^2}{\gamma(2-\gamma)}c_i^n, \quad i = 1, 2, \tag{17}$$
$$\frac{\partial}{\partial x}\left(\epsilon\frac{\partial\phi^{n+1,l+1}}{\partial x}\right) = -\chi_2\left(\rho_0 + \sum_{i=1}^2 z_i c_i^{n+1,l+1}\right),$$

for $l = 0, 1, 2, \ldots$, where $f(c_i, \phi)$ is defined as the right-hand side of (13)

$$f(c_i, \phi) = \frac{\partial}{\partial x}\left\{D_i\left[\frac{\partial c_i}{\partial x} + \chi_1\left(z_i c_i\frac{\partial\phi}{\partial x}\right)\right]\right\}. \tag{18}$$

We take $\gamma = 2 - \sqrt{2}$, which minimizes the local truncation error [11].

Removing the inner iterations, corresponding to the indices $k$ in (16) and $l$ in (17), Eqs. (16) and (17) is the TR-BDF2 scheme requiring a nonlinear solver for the two systems of nonlinear equations: (16) for $(c^{n+\gamma}, \phi^{n+\gamma})$ at the grid points and (17) for $(c^{n+1}, \phi^{n+1})$. With the inner iterations, Eqs. (16) and (17) provide a simple iterative scheme for solving the systems of nonlinear equations. For instance, at $k$-th iteration, we update the array $c^{n+\gamma,k+1}$ at the grid points by solving the first equation of (16) which is a tridiagonal system after the spatial discretization, since the values of $\phi^{n+\gamma,k}$ are known at $k$-th iteration; then, we update $\phi^{n+\gamma,k+1}$ using the second equation of (16). We perform the inner iterations until convergence and, as shown later, choosing two inner iterations $k = 2$ and $l = 2$ would be sufficient. As for initial guesses at the $n$-th time step, we choose

$\phi^{n+\gamma,0} = \phi^n$ for (16) and $\phi^{n+1,0} = \phi^{n+\gamma,k+1}$ for (17) with $k$ corresponding to the last inner iteration at the previous inner iteration. As shall be seen in Sect. 4, without any such inner iterations ($k = l = 0$), one could only attain first-order accuracy in time; on the other hand, with just one inner iteration ($k = l = 1$), one can attain second-order accuracy in time. In other words, the simple iterative scheme is very effective in solving the systems of nonlinear equations.

### 3.2 Discretization in space

Next, we provide the discrete equations for the spatial differential operators in Eqs. (16) and (17). Let's divide the dimensionless interval $[-1, 1]$ to $J$ subintervals, $x_j = -1 + j\Delta x$, where $\Delta x = 2/J$ and $j = 0, 1, \cdots, J$. We denote the numerical values of $g(x, t)$ at $(x_j, t_n)$ by $g_j^n$ and $g(x)$ at $x_j$ by $g_j$. We present the standard second-order central differencing schemes for the spatial differential operators here to facilitate the description of the mass-conservative scheme which depends on the details of the discretization at the interior grid points ($1 \le j \le J - 1$).

The ion diffusion term in Eq. (13) is discretized as

$$\frac{\partial}{\partial x}\left(D_i\frac{\partial c_i}{\partial x}\right)(x_j)$$
$$\approx \frac{D_{i,j+\frac{1}{2}}c_{j+1} - (D_{i,j+\frac{1}{2}} + D_{i,j-\frac{1}{2}})c_{i,j} + D_{i,j-\frac{1}{2}}c_{i,j-1}}{(\Delta x)^2}. \tag{19}$$

The term driven by the electrostatic potential gradient in Eq. (13) is given by

$$\frac{\partial}{\partial x}\left(D_i c_i\frac{\partial\phi}{\partial x}\right)(x_j)$$
$$\approx \frac{D_{i,j+1}c_{i,j+1}(\phi_{j+2} - \phi_j) - D_{i,j-1}c_{i,j-1}(\phi_j - \phi_{i,j-2})}{4(\Delta x)^2}. \tag{20}$$

The Laplacian in the Poisson equation (14) is approximated by

$$\frac{\partial}{\partial x}\left(\epsilon\frac{\partial\phi}{\partial x}\right)(x_j)$$
$$\approx \frac{1}{(\Delta x)^2}\left[\epsilon_{j+\frac{1}{2}}\phi_{j+1} - (\epsilon_{j+\frac{1}{2}} + \epsilon_{j-\frac{1}{2}})\phi_j + \epsilon_{j-\frac{1}{2}}\phi_{j-1}\right]. \tag{21}$$

The fully discretized form of (18) can be expressed as the matrix form $F_i(\phi)c_i$, where the nonzero entries of the tridi-

agonal matrix $F_i(\phi)$ are given by

$$
F_i(\phi)_{j,k} = \begin{cases} \frac{1}{\Delta x^2}(D_{i,j-\frac{1}{2}} - \chi_1 z_i D_{i,j-1} \frac{\phi_j - \phi_{j-2}}{4}) \\ \quad \text{for } k = j-1 \\ -\frac{1}{\Delta x^2}(D_{i,j+\frac{1}{2}} + D_{i,j-\frac{1}{2}}) \\ \quad \text{for } k = j \\ \frac{1}{\Delta x^2}(D_{i,j+\frac{1}{2}} + \chi_1 z_i D_{i,j+1} \frac{\phi_{j+2} - \phi_j}{4}) \\ \quad \text{for } k = j+1 \end{cases} \quad (22)
$$

and the vector $c_i = (c_{i,0}, c_{i,1}, \cdots, c_{i,J})^T$ denotes the unknown concentration at the grid points for the $i$-th ion species.

We can then write the fully discretized system as
(1) TR step:

$$
\left(I - \gamma \frac{\Delta t_n}{2} F_i(\phi^{n+\gamma})\right) c_i^{n+\gamma}
$$

$$
= \left(I + \gamma \frac{\Delta t_n}{2} F_i(\phi^n)\right) c_i^n, \quad \text{for } i = 1, 2, \quad (23)
$$

$$
G\phi^{n+\gamma} = -\left(\frac{\rho_0 L^2}{\phi_0 \epsilon_t} + \chi_2 \sum_{i=1}^{2} z_i c_i^{n+\gamma}\right),
$$

(2) BDF2 step:

$$
\left(I - \frac{1-\gamma}{2-\gamma} \Delta t_n F_i(\phi^{n+1})\right) c_i^{n+1}
$$

$$
= \frac{1}{\gamma(2-\gamma)} c_i^{n+\gamma} - \frac{(1-\gamma)^2}{\gamma(2-\gamma)} c_i^n, \quad i = 1, 2, \quad (24)
$$

$$
G\phi^{n+1} = -\left(\frac{\rho_0 L^2}{\phi_0 \epsilon_t} + \chi_2 \sum_{i=1}^{2} z_i c_i^{n+1}\right),
$$

where $G\phi$ provides the matrix form of the right-hand side of (21).

## 3.3 Discretization of boundary condition

We shall implement the boundary conditions using two different schemes. The first scheme is obtained by applying standard finite differencing to the boundary conditions, and the second is obtained by requiring the conservation of ions within the channel. As shown later, it is critical to preserve the ion concentrations for accurate numerical solutions.

### 3.3.1 Standard implementation

Applying the forward differencing to the right-hand side of the Nernst–Planck equation (13) at the left boundary and using the no-flux boundary condition in (15), we obtain

$$
\frac{\partial}{\partial x}\left\{D_i\left[\frac{\partial c_i}{\partial x} + \chi_1\left(z_i c_i \frac{\partial \phi}{\partial x}\right)\right]\right\}(-L)
$$

$$
\approx \frac{D_{i,1}[\frac{c_{i,2} - c_{i,0}}{2\Delta x} + \chi_1 z_i c_{i,1} \frac{\phi_2 - \phi_0}{2\Delta x}] - 0}{\Delta x}
$$

$$
= D_{i,1} \frac{c_{i,2} - c_{i,0} + \chi_1 z_i c_{i,1}(\phi_2 - \phi_0)}{2(\Delta x)^2}. \quad (25)
$$

It is similar at the right boundary. We implement the Robin boundary condition in (15) with the second-order central differencing using ghost grid points as

$$
(\phi_0 - \phi_-) - \eta \frac{\phi_1 - \phi_{-1}}{2\Delta x} = 0, \quad \text{or}
$$

$$
\phi_{-1} = \phi_1 - \frac{2\Delta x}{\eta}(\phi_0 - \phi_-), \quad (26)
$$

and similarly $\phi_{J+1} = \phi_{J-1} - \frac{2\Delta x}{\eta}(\phi_J - \phi_+)$.

### 3.3.2 Conservative scheme: TR step

The no-flux boundary condition in (15) implies that the total concentration of each ion species is constant throughout time. Thus, we discretize the equations by requiring the numerical value of the total concentration be conserved exactly in time.

First, we approximate the total concentration $c_{i,tot}(t_n)$ defined in Eq. (7) using the trapezoidal rule as follows

$$
c_{i,tot}^n = \sum_{j=1}^{J-1} c_{i,j}^n \Delta x + \frac{\Delta x}{2}\left(c_{i,0}^n + c_{i,J}^n\right) \quad (27)
$$

Let us examine the change of the total concentration in the TR step (23).

$$
\frac{c_{i,tot}^{n+\gamma} - c_{i,tot}^n}{\gamma \Delta t}
$$

$$
= \sum_{j=1}^{J-1} \frac{c_{i,j}^{n+\gamma} - c_{i,j}^n}{\gamma \Delta t} \Delta x
$$

$$
+ \frac{\Delta x}{2}\left(\frac{c_{i,0}^{n+\gamma} - c_{i,0}^n}{\gamma \Delta t} + \frac{c_{i,J}^{n+\gamma} - c_{i,J}^n}{\gamma \Delta t}\right)
$$

$$
= \sum_{j=1}^{J-1}\left[\frac{D_{i,j+\frac{1}{2}} c_{i,j+1}^{n+\gamma} - (D_{i,j+\frac{1}{2}} + D_{i,j-\frac{1}{2}}) c_{i,j}^{n+\gamma}}{2\Delta x}\right.
$$

$$
+ \frac{D_{i,j-\frac{1}{2}} c_{i,j-1}^{n+\gamma}}{2\Delta x} + \chi_1 z_i \frac{D_{i,j+1} c_{i,j+1}^{n+\gamma}(\phi_{j+2}^n - \phi_j^n)}{8\Delta x}
$$

$$
- \chi_1 z_i \frac{D_{i,j-1} c_{i,j-1}^{n+\gamma}(\phi_j^n - \phi_{j-2}^n)}{8\Delta x}
$$

$$
+ \frac{D_{i,j+\frac{1}{2}} c_{i,j+1}^n - (D_{i,j+\frac{1}{2}} + D_{i,j-\frac{1}{2}}) c_{i,j}^n}{2\Delta x}
$$

$$+ \frac{D_{i,j-\frac{1}{2}} c_{i,j-1}^n}{2\Delta x} + \chi_1 z_i \frac{D_{i,j+1} c_{i,j+1}^n (\phi_{j+2}^n - \phi_j^n)}{8\Delta x}$$

$$- \chi_1 z_i \frac{D_{i,j-1} c_{i,j-1}^n (\phi_j^n - \phi_{j-2}^n)}{8\Delta x} \Bigg]$$

$$+ \frac{\Delta x}{2} \left( \frac{c_{i,0}^{n+\gamma} - c_{i,0}^n}{\gamma \Delta t} + \frac{c_{i,J}^{n+\gamma} - c_{i,J}^n}{\gamma \Delta t} \right). \tag{28}$$

This summation has a telescoping effect where most of the interior terms cancel each other and we are left with

$$\frac{c_{i,tot}^{n+\gamma} - c_{i,tot}^n}{\gamma \Delta t}$$

$$= \frac{\Delta x}{2} \left( \frac{c_{i,0}^{n+\gamma} - c_{i,0}^n}{\gamma \Delta t} + \frac{c_{i,J}^{n+\gamma} - c_{i,J}^n}{\gamma \Delta t} \right)$$

$$+ \frac{D_{i,\frac{1}{2}}(c_{i,0}^{n+\gamma} + c_{i,0}^n - c_{i,1}^{n+\gamma} - c_{i,1}^n)}{2\Delta x}$$

$$+ \frac{D_{i,J-\frac{1}{2}}(c_{i,J}^{n+\gamma} + c_{i,J}^n - c_{i,J-1}^{n+\gamma} - c_{i,J-1}^n)}{2\Delta x}$$

$$- \chi_1 z_i \frac{D_{i,0}(c_{i,0}^{n+\gamma} + c_{i,0}^n)(\phi_1^n - \phi_{-1}^n)}{8\Delta x}$$

$$- \chi_1 z_i \frac{D_{i,1}(c_{i,1}^{n+\gamma} + c_{i,1}^n)(\phi_2^n - \phi_0^n)}{8\Delta x}$$

$$+ \chi_1 z_i \frac{D_{i,J-1}(c_{i,J-1}^{n+\gamma} + c_{i,J-1}^n)(\phi_J^n - \phi_{J-2}^n)}{8\Delta x}$$

$$+ \chi_1 z_i \frac{D_{i,J}(c_{i,J}^{n+\gamma} + c_{i,J}^n)(\phi_{J+1}^n - \phi_{J-1}^n)}{8\Delta x}. \tag{29}$$

We can achieve the conservation of the total concentration $c_{i,tot}^{n+\gamma} = c_{i,tot}^n$, if we discretize the Nernst–Planck equation (13) at the left boundary as

$$\frac{c_{i,0}^{n+\gamma} - c_{i,0}^n}{\gamma \Delta t}$$

$$= \frac{D_{i,\frac{1}{2}}(c_{i,1}^{n+\gamma} - c_{i,0}^{n+\gamma} + c_{i,1}^n - c_{i,0}^n)}{(\Delta x)^2}$$

$$+ \chi_1 z_i \frac{D_{i,0}(c_{i,0}^{n+\gamma} + c_{i,0}^n)(\phi_1^n - \phi_{-1}^n)}{4(\Delta x)^2}$$

$$+ \chi_1 z_i \frac{D_{i,1}(c_{i,1}^{n+\gamma} + c_{i,1}^n)(\phi_2^n - \phi_0^n)}{4(\Delta x)^2}, \tag{30}$$

and at the right boundary as

$$\frac{c_{i,J}^{n+\gamma} - c_{i,J}^n}{\gamma \Delta t}$$

$$= - \frac{D_{i,J-\frac{1}{2}}(c_{i,J}^{n+\gamma} - c_{i,J-1}^{n+\gamma} + c_{i,J}^n - c_{i,J-1}^n)}{(\Delta x)^2}$$

$$- \chi_1 z_i \frac{D_{i,J-1}(c_{i,J-1}^{n+\gamma} + c_{i,J-1}^n)(\phi_J^n - \phi_{J-2}^n)}{4(\Delta x)^2}$$

$$- \chi_1 z_i \frac{D_{i,J}(c_{i,J}^{n+\gamma} + c_{i,J}^n)(\phi_{J+1}^n - \phi_{J-1}^n)}{4(\Delta x)^2}. \tag{31}$$

It is important to point out that Eq. (30) can be seen as discretizing equation (13) using a first-order finite difference with grid size $\Delta x/2$ and using the no-flux boundary condition (15). Equation (30) can be rewritten as

$$\frac{c_{i,0}^{n+\gamma} - c_{i,0}^n}{\gamma \Delta t} = \frac{[D_{i,\frac{1}{2}}(c_{i,1}^{n+\gamma} - c_{i,0}^{n+\gamma})/\Delta x + \frac{\chi_1 z_i}{2}(D_{i,0} c_{i,0}^{n+\gamma} \frac{\phi_1^n - \phi_{-1}^n}{2\Delta x} + D_{i,1} c_{i,1}^{n+\gamma} \frac{\phi_2^n - \phi_0^n}{2\Delta x})] - 0}{\Delta x}$$

$$+ \frac{[D_{i,\frac{1}{2}}(c_{i,1}^n - c_{i,0}^n)/\Delta x + \frac{\chi_1 z_i}{2}(D_{i,0} c_{i,0}^n \frac{\phi_1^n - \phi_{-1}^n}{2\Delta x} + D_{i,1} c_{i,1}^n \frac{\phi_2^n - \phi_0^n}{2\Delta x})] - 0}{\Delta x}$$

$$\approx \frac{\frac{1}{2}[(D_i \frac{\partial c_i^{n+\gamma}}{\partial x} + \chi_1 z_i D_i c_i^{n+\gamma} \frac{\partial \phi^n}{\partial x})(x_{\frac{1}{2}}) + (D_i \frac{\partial c_i^n}{\partial x} + \chi_1 z_i D_i c_i^n \frac{\partial \phi^n}{\partial x})(x_{\frac{1}{2}})] - 0}{\Delta x/2}. \tag{32}$$

### 3.3.3 Conservative scheme: BDF2 step

We can rewrite Eq. (24) in such a way that the numerical value of the derivative of the total concentration becomes a linear combination of the result from the TR step and the

right hand side of Eq. (13) evaluated at the $n + 1$th time step.

$$\frac{c_j^{n+1} - c_j^{n+\gamma}}{(1-\gamma)\Delta t} = \frac{1-\gamma}{2-\gamma} \frac{c_j^{n+\gamma} - c_j^n}{\gamma \Delta t} + \frac{1}{2-\gamma} f(c_j^{n+1}) \tag{33}$$

As with the TR step, almost all of the interior terms cancel in a telescoping sum, and we can require the exact conservation of the total concentration $c_{i,tot}^{n+1} = c_{i,tot}^{n+\gamma}$ in order to obtain the discretization of the Nernst–Planck equation (13) at the boundaries for the BDF2 step:

$$
\frac{c_{i,0}^{n+1} - c_{i,0}^{n+\gamma}}{(1-\gamma)\Delta t}
$$

$$
= \frac{1-\gamma}{2-\gamma}\left(\frac{c_{i,0}^{n+\gamma} - c_{i,0}^n}{\gamma\Delta t}\right)
$$

$$
+ \frac{2}{2-\gamma}\frac{D_{i,\frac{1}{2}}(c_{i,1}^{n+1} - c_{i,0}^{n+1})}{(\Delta x)^2}
$$

$$
+ \frac{\chi_1 z_i}{2-\gamma}\frac{D_{i,0}c_{i,0}^{n+1}(\phi_1^n - \phi_{-1}^n) + D_{i,1}c_{i,1}^{n+1}(\phi_2^n - \phi_0^n)}{2(\Delta x)^2},
$$
(34)

$$
\frac{c_{i,J}^{n+1} - c_{i,J}^{n+\gamma}}{(1-\gamma)\Delta t}
$$

$$
= \frac{1-\gamma}{2-\gamma}\left(\frac{c_{i,J}^{n+\gamma} - c_{i,J}^n}{\gamma\Delta t}\right)
$$

$$
- \frac{2}{2-\gamma}\frac{D_{i,J-\frac{1}{2}}(c_{i,J}^{n+1} - c_{i,J-1}^{n+1})}{(\Delta x)^2}
$$

$$
- \frac{\chi_1 z_i}{2-\gamma}\frac{D_{i,J-1}c_{i,J-1}^{n+1}(\phi_J^n - \phi_{J-2}^n)}{2(\Delta x)^2}
$$

$$
- \frac{\chi_1 z_i}{2-\gamma}\frac{D_{i,J}c_{i,J}^{n+1}(\phi_{J+1}^n - \phi_{J-1}^n)}{2(\Delta x)^2}.
$$
(35)

Equation (34) can be seen as discretizing only the term $f(c_{i,j}^{n+1})$ in Eq. (24) using forward difference with grid size $\Delta x/2$ and using the no-flux boundary condition in (15). Equation (35) can be viewed similarly at the right boundary.

### 3.4 Positivity-preserving conditions

The ion concentrations governed by the PNP equations are always positive or non-negative at any point in space and for all times. The numerical solution to (23) and (24) does not necessarily guarantee to preserve positivity property of the solution. In this section, we derive a set of conditions, (44a) and (44b), on the time and space step sizes to ensure that the solution be always non-negative at every point.

First, by factoring and simplifying, we combine the TR step (23) and BDF2 step (24) into the following compact form

$$
\left(I - \frac{\gamma\Delta t}{2}F(\phi^{n+\gamma})\right)\left(I - \frac{1-\gamma}{2-\gamma}\Delta t F(\phi^{n+1})\right)c^{n+1}
$$

$$
= \left(I + \frac{\Delta t}{2(2-\gamma)}\left(F(\phi^n) + (1-\gamma)^2 F(\phi^{n+\gamma})\right)\right)c^n,
$$
(36)

where the matrices $F$ are defined in (22). Here and in this section, we have dropped the subscript $i$ for convenience of presentation. We can analyze this in steps to find the conditions under which the system is positivity-preserving. We assume the gradient of the potential, $|\frac{\partial\phi}{\partial x}|$, is bounded. Consequently, we denote the bound for its finite difference approximations by

$$
D_\phi := \max_{i,j,n}\left|\frac{z_i(\phi_{j+1}^n - \phi_{j-1}^n)}{2\Delta x}\right|
$$
(37)

**Lemma 1** *All matrix equations of the form $(I - kF(\phi))c^* = \tilde{c}$ preserve positivity for any $k > 0$, where $F$ is defined in (22), i.e., $c^* > 0$ (all elements of $c^*$ are positive) provided that $\tilde{c} > 0$.*

*Proof* This is a consequence of Lemma I.7.4 of [18]. If we can show that the conditions (I.7.14) and (I.7.15) of [18] are satisfied, then the positivity is preserved. Consider the forward Euler scheme

$$
c^{**} = (I + kF(\phi))\tilde{c}.
$$
(38)

First, we show that $c^{**}$ is conditionally positive given all entries of $\tilde{c}$ are positive ($\tilde{c}_j > 0 \, \forall j$), i.e.,

$$
0 \le \tilde{c}_j + k\frac{D_{j+\frac{1}{2}}\tilde{c}_{j+1} - (D_{j+\frac{1}{2}} + D_{j-\frac{1}{2}})\tilde{c}_j + D_{j-\frac{1}{2}}\tilde{c}_{j-1}}{(\Delta x)^2} + k\chi_1 z_i\frac{D_{j+1}\tilde{c}_{j+1}(\phi_{j+2} - \phi_j) - D_{j-1}\tilde{c}_{j-1}(\phi_j - \phi_{j-2})}{4(\Delta x)^2}
$$

To get the coefficients of $\tilde{c}_j$ terms to be positive, we need

$$
1 - (D_{j+\frac{1}{2}} + D_{j-\frac{1}{2}})\frac{k}{\Delta x^2} \ge 0
$$
(39)

or

$$
1 - (2D_{\max})\frac{k}{\Delta x^2} \ge 0, \quad \text{i.e. } k\frac{2D_{\max}}{\Delta x^2} \le 1,
$$
(40)

where

$$D_{\max} = \max_{i,j} D_{i,j}, \qquad D_{\min} = \min_{i,j} D_{i,j} \qquad (41)$$

are the maximum and the minimum of the diffusion coefficients respectively. In order to guarantee the terms involving $c_{j+1}, c_{j-1}$ be positive, we impose

$$\frac{D_{j+1/2}}{\Delta x^2} + \frac{D_{j+1}\chi_1 z_i}{2\Delta x}\frac{\phi_{j+2} - \phi_j}{2\Delta x} \geq 0, \qquad (42a)$$

and

$$\frac{D_{j-1/2}}{\Delta x^2} - \frac{D_{j-1}\chi_1 z_i}{2\Delta x}\frac{\phi_j - \phi_{j-2}}{2\Delta x} \geq 0 \qquad (42b)$$

to be true for all $i, j$. We can thus guarantee positivity by

$$\frac{D_{\min}}{\Delta x^2} - \frac{D_{\max}\chi_1 D_\phi}{2\Delta x} \geq 0, \quad \text{i.e. } \Delta x \leq \frac{2D_{\min}}{D_{\max}\chi_1 D_\phi}, \qquad (43)$$

where $D_\phi$, $D_{\max}$ and $D_{\min}$ are defined in (37) and (41) respectively. Therefore, if we assume the system of equations $(I - kF(\phi))c^* = \tilde{c}$ is solvable, by Lemma I.7.4 of [18], we have proved that $c^*$ is positive for any $k > 0$. □

With Lemma 1, we are ready to show the positivity-preserving property of our scheme (36) as follows. First, similar to the proof of Lemma 1, one can show that the right-hand side (36), denoted by $c^{n,*}$, preserves positivity if the following conditions are satisfied

$$\frac{\Delta t}{\Delta x^2} \leq \frac{2 - \gamma}{(1 + (1 - \gamma)^2)D_{\max}} \qquad (44a)$$

and

$$\Delta x \leq \frac{2D_{\min}}{D_{\max}\chi_1 D_\phi}. \qquad (44b)$$

Next, the matrix equation (36)

$$\left(I - \frac{\gamma\Delta t}{2}F(\phi^{n+\gamma})\right)\left(I - \frac{1-\gamma}{2-\gamma}\Delta t F(\phi^{n+1})\right)c^{n+1}$$
$$= c^{n,*} \qquad (45)$$

is equivalent to the following two equations of the form in Lemma 1

$$\left(I - \frac{\gamma\Delta t}{2}F(\phi^{n+\gamma})\right)c^{n,**} = c^{n,*}, \qquad (46a)$$

$$\left(I - \frac{1-\gamma}{2-\gamma}\Delta t F(\phi^{n+1})\right)c^{n+1} = c^{n,**}. \qquad (46b)$$

Finally, applying Lemma 1 to each of the Eqs. (46a) and (46b), we have shown that, if the conditions (44a) and (44b) are satisfied, our numerical scheme (36) is positivity-preserving.

## 4 Numerical results

### 4.1 Validation and convergence results

To validate the accuracy our numerical method, we compare the steady-state solution from our dynamic simulations of PNP with that of the Poisson–Boltzmann solution taken from the work [21]. Figure 1 shows that our steady-state solutions match perfectly with those in [21] for two sets of parameters: one with $\eta = \epsilon = 2^{-2}$ and the other $\eta = \epsilon = 2^{-6}$ while keeping the other parameters constant: $\phi_- = -1$, $\phi_+ = 1$, $D_1 = D_2 = 1$, $\chi_1 = 1$, $\chi_2 = \frac{1}{2\epsilon}$, and $\rho_0 = 0$. The maximum difference in $\phi$ between the two solutions is less than $5.6 \times 10^{-5}$. To get the steady-state solution, we have used the mass-conservative TR-BDF2 method described in previous sections with 2048 grid points in the interval $[-1, 1]$ as in [21] and the time-step size $10^{-4}$. At time $t = 0$, the initial profiles for the ion concentrations are uniform in space. In this case, our time-dependent solution is close to the steady-state solution for the time $t \geq 2$. We have also verified that our solutions agree with those in [21] for other sets of parameters as well, although they are not shown here.

We have also checked the orders of convergence of our methods. The discretization method described in the previous section always has $O(\Delta x^2)$ convergence in space, regardless whether we have implemented the mass-conservative difference scheme or not. The order of convergence in space is computed using the formula $\log_2 \frac{|\Phi(2\Delta x) - \Phi(4\Delta x)|}{|\Phi(\Delta x) - \Phi(2\Delta x)|}$, where $\Phi(\Delta x)$ denotes the numerical solution of the potential $\phi$ at the point $(x, t) = (0.904, 0.02)$ obtained with spatial resolution $\Delta x$. In this case, the time step size is chosen to be very small $\Delta t = 10^{-6}$ so that the discretization error is dominated by that in space.
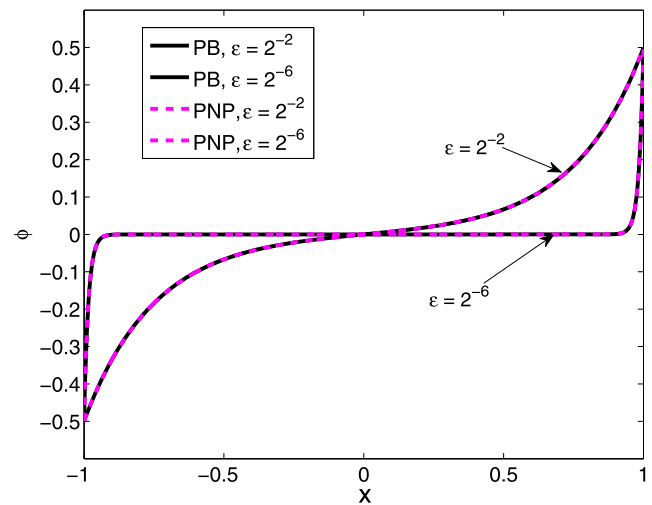


**Fig. 1** Comparing our steady-state solution (the *dashed lines*) using TR-BDF2 method with that of the Poisson–Boltzmann equation (the *solid lines*) obtained in [21]. The parameters are $\epsilon = 2^{-2}, 2^{-6}$, $\eta = \epsilon$, $\phi_- = -1$, $\phi_+ = 1$

**Table 1** The numerical order of convergence in time for the mass-conservative TR-BDF2 method solving the PNP equations in one dimension for two ion species. The non-dimensionalized physical parameters are $\epsilon = 1$, $\eta = 4.63 \times 10^{-5}$, $\phi_- = 1$, $\phi_+ = -1$. The calculations are performed with $\Delta x = 0.002$ and the numerical solution of $\phi$ is evaluated at the point $(x, t) = (0.904, 0.02)$

| $\Delta t$ | $5 \times 10^{-5}$ | $2.5 \times 10^{-5}$ | $1.25 \times 10^{-5}$ |
|---|---|---|---|
| Order of convergence for TR-BDF2, no inner loops | 1.0016 | 1.0008 | 1.0028 |
| Order of convergence for TR-BDF2, two inner loops | 2.2197 | 2.1779 | 2.2143 |

To obtain the numerical orders of convergence in time, we compute the numerical solutions with three different time-step sizes $\Delta t, 2\Delta t$ and $4\Delta t$ and then calculate the numerical order of convergence $p$ by computing the ratio $(\Phi(2\Delta t) - \Phi(4\Delta t))/(\Phi(\Delta t) - \Phi(2\Delta t))$ at the fixed position and time $(x, t) = (0.904, 0.02)$. Here, the spatial resolutions in these simulations are kept the same, $\Delta x = 0.002$. The numerical convergence results in time are given in Table 1. We find that, if one did not perform inner iterations ($k = 0$ in (23) and $l = 0$ in (24)), the convergence of TR-BDF2 would be first-order in time. If we include at least one inner iteration ($k \geq 1$ and $l \geq 1$), then the convergence becomes second-order as expected.

### 4.2 Evolution of the distributions of the ions

First, we examine the evolution of the ion concentrations and the electrostatic potential starting from a uniform ion distribution of two ion species of opposite valence $z_1 = 1$ and $z_2 = -1$: $c_i(x, 0) = 1$, $i = 1, 2$, for $-1 \leq x \leq 1$. The prescribed electrostatic potentials on the left and the right at far-field are $\phi_- = 1$ and $\phi_+ = -1$ respectively. The physical parameters are specified as in Sect. 2.3. In the rest of this work, unless we specify otherwise, the non-dimensionalized parameters are chosen as $D_1 = D_2 = 1$, $\chi_1 = 3.1$, $\chi_2 = 125.4$ and $\eta = 4.63 \times 10^{-5}$, as they were defined in Sect. 2.3. Due to the symmetries of the initial and boundary conditions, the parameters and the domain, the profiles for the concentrations of the two ion species at any time are symmetric with respect to the center of the channel, $x = 0$.

Figure 2 shows the profiles of the ion concentration with the valence $z_2 = -1$ and the electrostatic potential at the times $t = 0, 0.01, 0.05$, and 1. The Robin boundary condition (15) for the electrostatic potential drives the ions with negative charges toward the left boundary and the no-flux boundary condition (15) for the ions causes those charges to accumulate at the boundary. In this case, the ion concentrations keep their uniform profile in the bulk of the domain away from the two ends, while the electrostatic potential changes from an initially linear profile to one that is essentially constant (zero) except for the sharp gradient at each
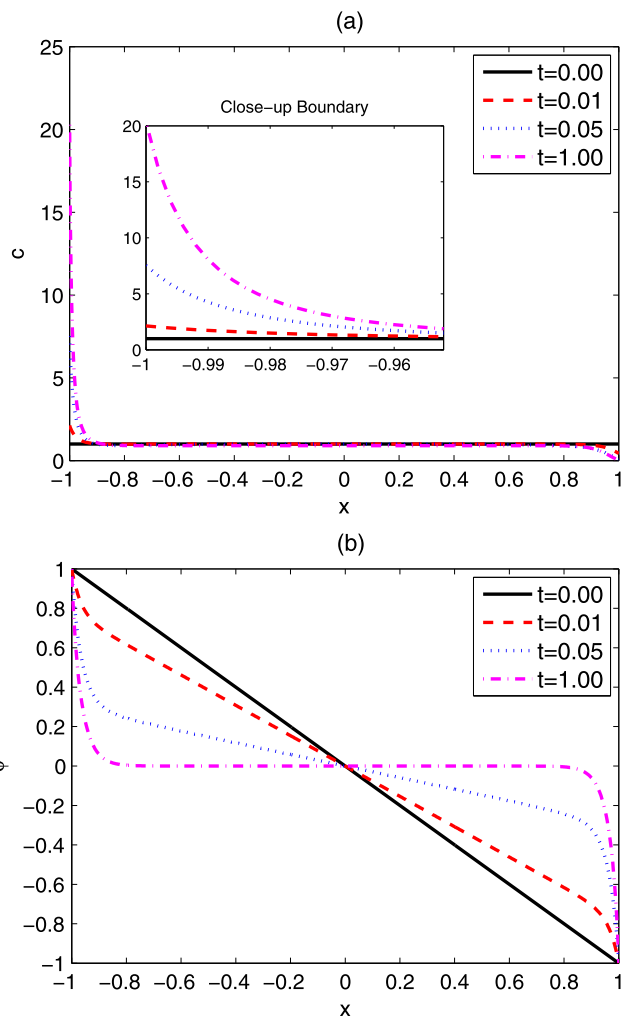


**Fig. 2** Simulation results using the mass-conservative TR-BDF2 method for $\epsilon = 1$, $\eta = 4.63 \times 10^{-5}$, $\phi_- = 1$, $\phi_+ = -1$. The calculations were performed with $\Delta t = 10^{-4}$ and $\Delta x = 0.002$. (**a**) The concentration profiles for the ion species with the valence $z_2 = -1$, $c_2(x, t)$, are plotted at the times $t = 0$ (the *solid line*), 0.01 (*dashed*), 0.05 (*dotted*) and 1 (*dash-dotted*). (**b**) The corresponding time sequence of the electrostatic potential $\phi$ is plotted

end. We find that the existence of the thin boundary layers requires high spatial resolution or small $\Delta x$ in the simulation. The numerical results would be far away from the correct solution if we chose $\Delta x > 0.05$. These results show the overall behavior of the system as time elapses.

### 4.3 Comparison between mass-conservative and standard schemes

Next, let us compare the numerical results from a standard discretization (called as the non-conservative schemes) of the boundary conditions, (25), with those obtained from the mass-conservative schemes (30) and (34). Figure 3 shows the ion concentration profiles and the electrostatic potential at time $t = 1$ obtained from both the mass-conservative
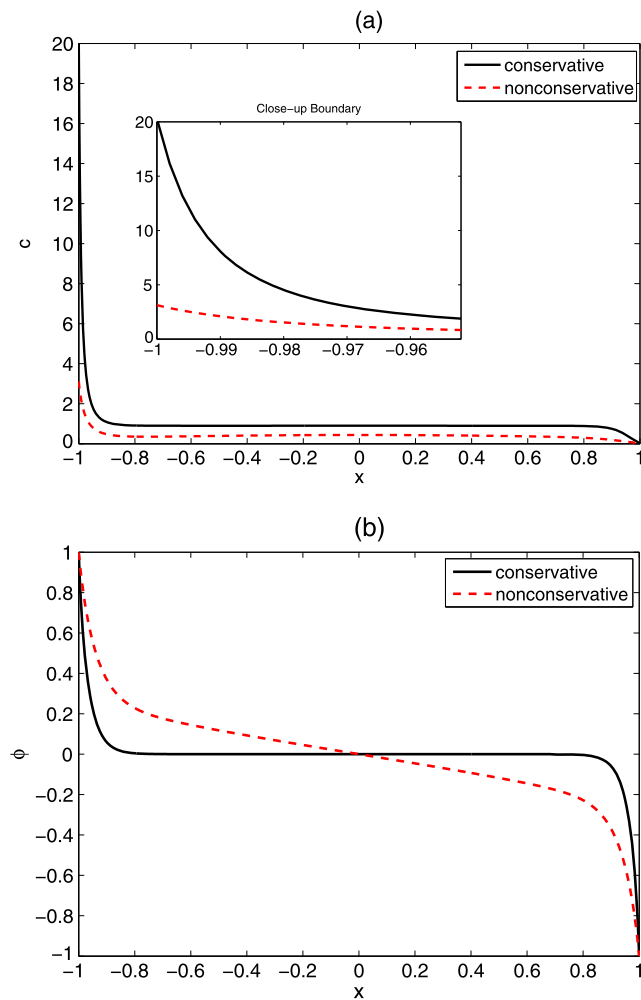
Fig. 3 Comparison between the simulation results from the mass-conservative and the non-conservative schemes for $\epsilon = 1$, $\eta = 4.63 \times 10^{-5}$, $\phi_- = 1$, $\phi_+ = -1$, $T = 1$. The calculations were performed with $\Delta t = 10^{-4}$ and $\Delta x = 0.002$. (a) The ion concentration profiles of $c_2$ from the mass-conservative method (the *solid line*) and the non-conservative method (the *dashed line*). (b) The corresponding electrostatic potentials



Fig. 4 (a) The total ion concentration for species 2 as a function of time from the simulations using the mass-conservative (*solid*) and non-conservative (*dashed*) schemes. (b) The relative error in total concentration for both species. The parameters are identical to those in Fig. 3

schemes (the solid lines) and the non-conservative schemes (the dashed lines). The parameters in the computations are the same as described in the previous Sect. 4.2. To make fair comparison, all other aspects are kept same, including the time-step scheme (TR-BDF2), the discretization scheme for interior points of the domain, the initial condition, the physical parameters, the time-step size $\Delta t$ and the space resolution $\Delta x$. As shown in Fig. 3(a), the ion concentration from the non-conservative scheme is substantially lower than that from the mass-conservative scheme and the variations near the boundaries are much smaller in the result from the non-conservative scheme. Furthermore, the electrostatic potential obtained from the non-conservative scheme, shown in Fig. 3(b), has a linear profile with non-zero slope in the middle of the domain and much milder slopes at the bound-
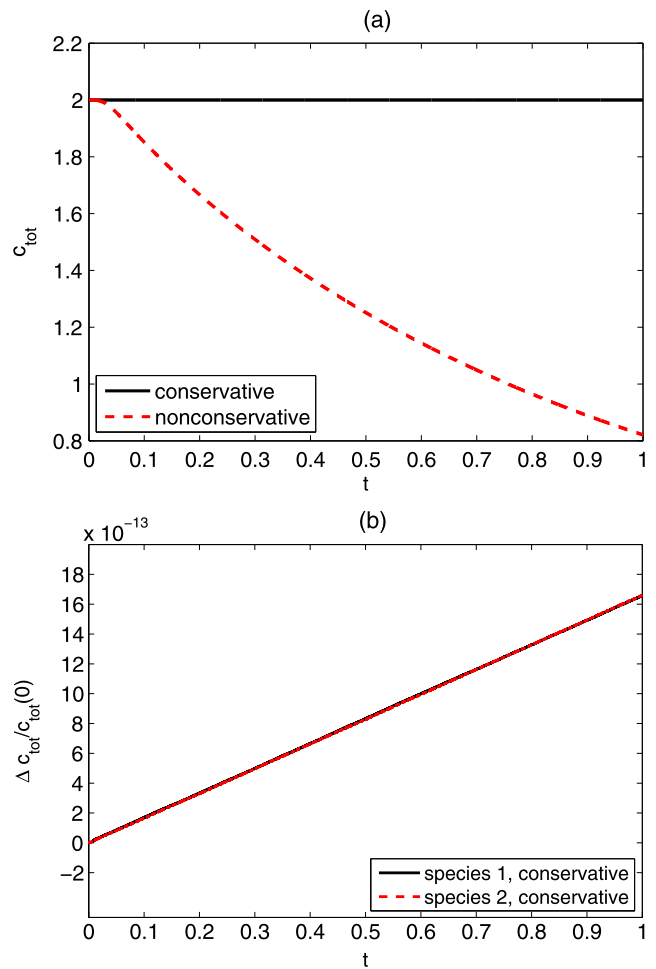
aries, when compared with that from the mass-conservative schemes.

Because of the no-flux boundary conditions (3a), the total concentration of each ion species should be invariant in time. Figure 4 shows that the mass-conservative scheme preserves the conservation of the ions perfectly (up to the level of roundoff error) over a long period of time, while the total number of ions at the time $t = 1$ obtained from the non-conservative scheme is reduced to less than half of the original amount.

Figure 5(a) shows that the total energy $E$ as a function of time $t$ for both the conservative and non-conservative schemes. The total energy obtained from the mass-conservative scheme approaches the minimum energy state much faster than that from the non-conservative scheme. More importantly, in Sect. 2.2, it is shown that the total energy of the system $E$ defined as (8) satisfies the energy dissipation law (10). In Fig. 5(b), we plot the rate of change in energy, $\frac{dE}{dt}$, for the mass-conservative (the solid line) and
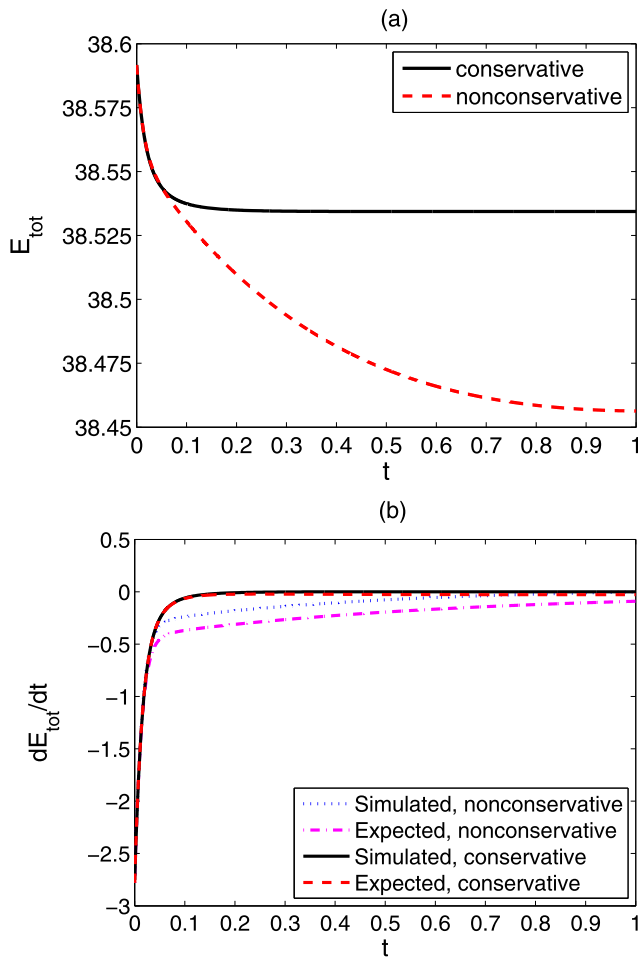
(a)

(b)

Fig. 5 (a) The total energy as a function of time from the simulations using the mass-conservative (*solid*) and non-conservative (*dashed*) schemes. (b) The rate of change in energy, $\frac{dE}{dt}$, obtained from the graph (a) and the right-hand side of Eq. (10). The *solid* and the *dotted lines* correspond to the left-hand side of Eq. (10) for the mass-conservative and the non-conservative schemes respectively. The *dashed* and the *dash-dotted lines* correspond to the right-hand side of Eq. (10) for the mass-conservative and the non-conservative schemes respectively. The parameters are identical to those in Fig. 3

the non-conservative schemes (the dotted line) obtained by using a second-order finite difference based on the numerical result $E(t)$ shown in Fig. 5(a). In the same graph, we also plot the expected dissipation rate given by the right-hand side of (10), computed using the second-order central differencing and trapezoidal rule and shown by the dashed line for the conservative scheme and the dash-dotted line for the non-conservative scheme in Fig. 5(b). It shows that the numerical result from the conservative scheme (the solid line) agrees with the energy dissipation law (the dashed line) very well. In contrast, the corresponding results for the non-conservative scheme show that the energy dissipation law is not satisfied after a short period of time. This is due to the fact that the total concentration from the non-conservative scheme displays very poor performance in conserving the
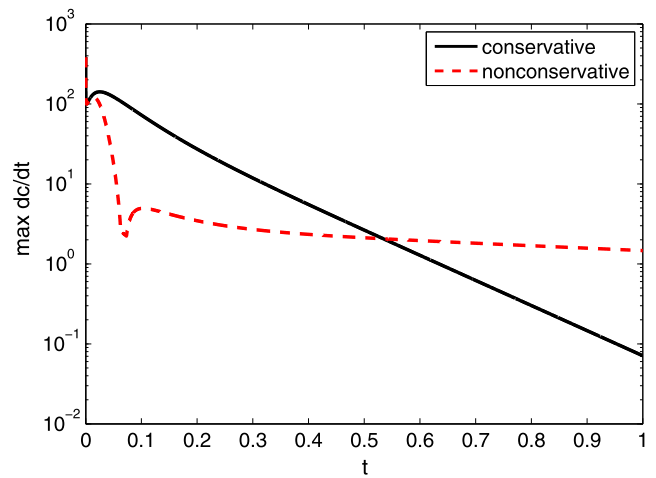


Fig. 6 The maximum rate of change in ion concentrations as a function of time for the non-conservative (the *dashed line*) and conservative (the *solid line*) schemes. The parameters are identical to those in Fig. 3

total concentrations. The results show that the discretization of the boundary conditions have profound impact on satisfying the physical properties: the energy dissipation law and the conservation of the total number of ions.

In addition to energy decay, we compute the maximum rate of change in the concentrations of the species over the domain, i.e. $\max_{i,-1\leq x\leq 1}|\frac{\partial c_i}{\partial t}|$. It is notable from the time derivative of concentration shown in Fig. 6 that the numerical results from the conservative numerical scheme steadily approach the equilibrium in time. On the other hand, the non-conservative scheme is approaching a steady state much faster initially, but, later in time, the non-conservative scheme's behavior changes and it does not appear to reach a steady state. This result emphasizes the necessity of the conservative numerical scheme for long-time simulation.

### 4.4 Effect of parameters

The size of the difference in the results from conservative and non-conservative schemes depends on the non-dimensional parameter $\chi_2 = \frac{ec_0L^2}{\phi_0\epsilon_t}$. For the physical model of the ion transportations, the value of $\chi_2$ can be arbitrarily large, depending on the values of average ion concentration $c_0$ and the applied electrostatic potential $\phi_0$ at the boundaries. Consequently, it is important to pay attention to the size of the dimensionless parameter $\chi_2$. In Fig. 3, we have shown that, for $\chi_2 = 125.4$, the results of non-conservative schemes are far away from the correct results. Figure 7(a) and (c) show the profiles of the electrostatic potential $\phi$ at a fixed time $t = 1$ from both the conservative and the non-conservative schemes with two more different values of $\chi_2 = 31.35$ and $501.6$, while keeping all other parameters the same as those for Fig. 3. At $t = 1$, the system has reached the steady state, shown by the constant values for the conser-
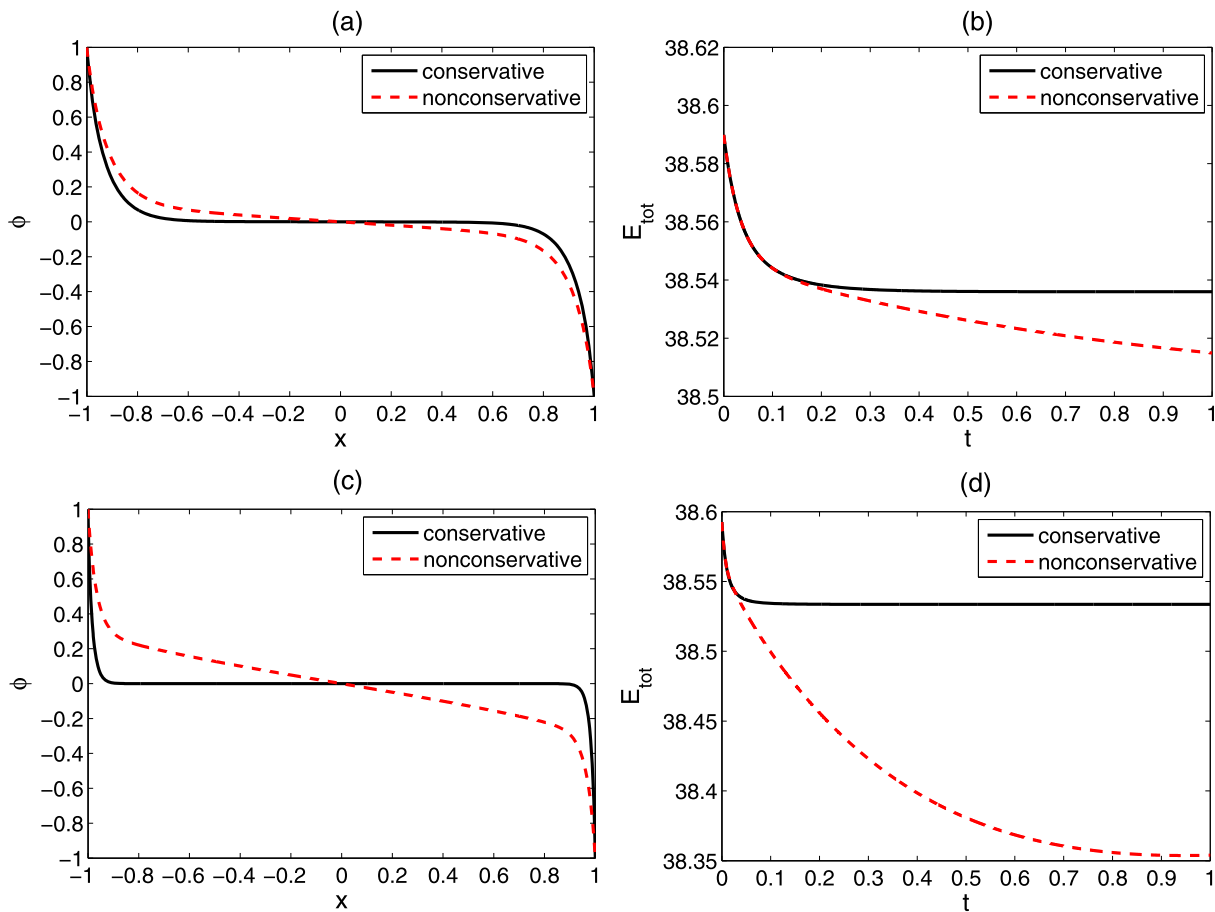
**Fig. 7** Comparison between the simulation results from the mass-conservative and the non-conservative schemes for different values of the non-dimensional parameter $\chi_2$. (**a**) The electric potential for the conservative and non-conservative schemes using $\chi_2 = 31.35$. (**b**) The total energy for the conservative and non-conservative schemes using $\chi_2 = 31.35$. (**c**) The electric potential for the conservative and non-conservative schemes using $\chi_2 = 501.60$. (**d**) The total energy for the conservative and non-conservative schemes using $\chi_2 = 501.60$. The calculations were performed with $\Delta t = 10^{-4}$ and $\Delta x = 0.001$. The other parameters are identical to those in Fig. 3

vative scheme in the energy plots of Fig. 7(b) and (d). Comparing the graphs of potential in Figs. 3(a), (c) and 7, we find that the value of $\chi_2$ primarily affects the width of the boundary layer, with larger $\chi_2$ resulting in thinner boundary layers. A thinner boundary layer transitions much more sharply near the boundaries, and thus requires more computational grid points in the region and more truthful discretization of the boundary conditions. This causes the differences in electrostatic potential profiles and the energy dissipation in time (shown by Fig. 7(b) and (d)) between the conservative and non-conservative schemes to be greater as one increases $\chi_2$. A thinner boundary layer also affects performance with regard to the energy dissipation law, which is not shown here in plots. Larger $\chi_2$ leads to a larger discrepancy between the decay rate of the total energy (the left-hand side of Eq. 10) and the energy dissipation rate (the right-hand side of the law Eq. 10), and this discrepancy gets worse faster for the non-conservative scheme than for the conservative scheme.

Finally, we examine the effect of the parameter $\eta$ in the Robin boundary condition (3b) on the numerical results. As noted in Sect. 4.1, the steady state changes dramatically if the relative values of the physical parameters $\eta$ and $\epsilon$ are changed. In order to determine the effect of $\eta$ itself on the results, we have tested a range of non-dimensionalized values for $\eta$ ranging from $10^{-6}$ to 1, while holding $\epsilon$ at its constant non-dimensionalized value of 1. We find that, when $\eta$ increases from $10^{-6}$ to 0.001, the concentration profiles at the steady state do not change much, having a maximum relative difference of only $10^{-4}$, but this property does not generalized to larger $\eta$. We also find that the discretization error, especially for the non-conservative scheme, is significantly affected by the value of $\eta$. For large values of $\eta$, say $\eta > 0.1$, the growth of the discretization error of the non-conservative scheme is rather slow, and consequently the concentration and electric potential profiles obtained from the non-conservative scheme are close to those obtained by the mass-conservative schemes. An example of this prop-
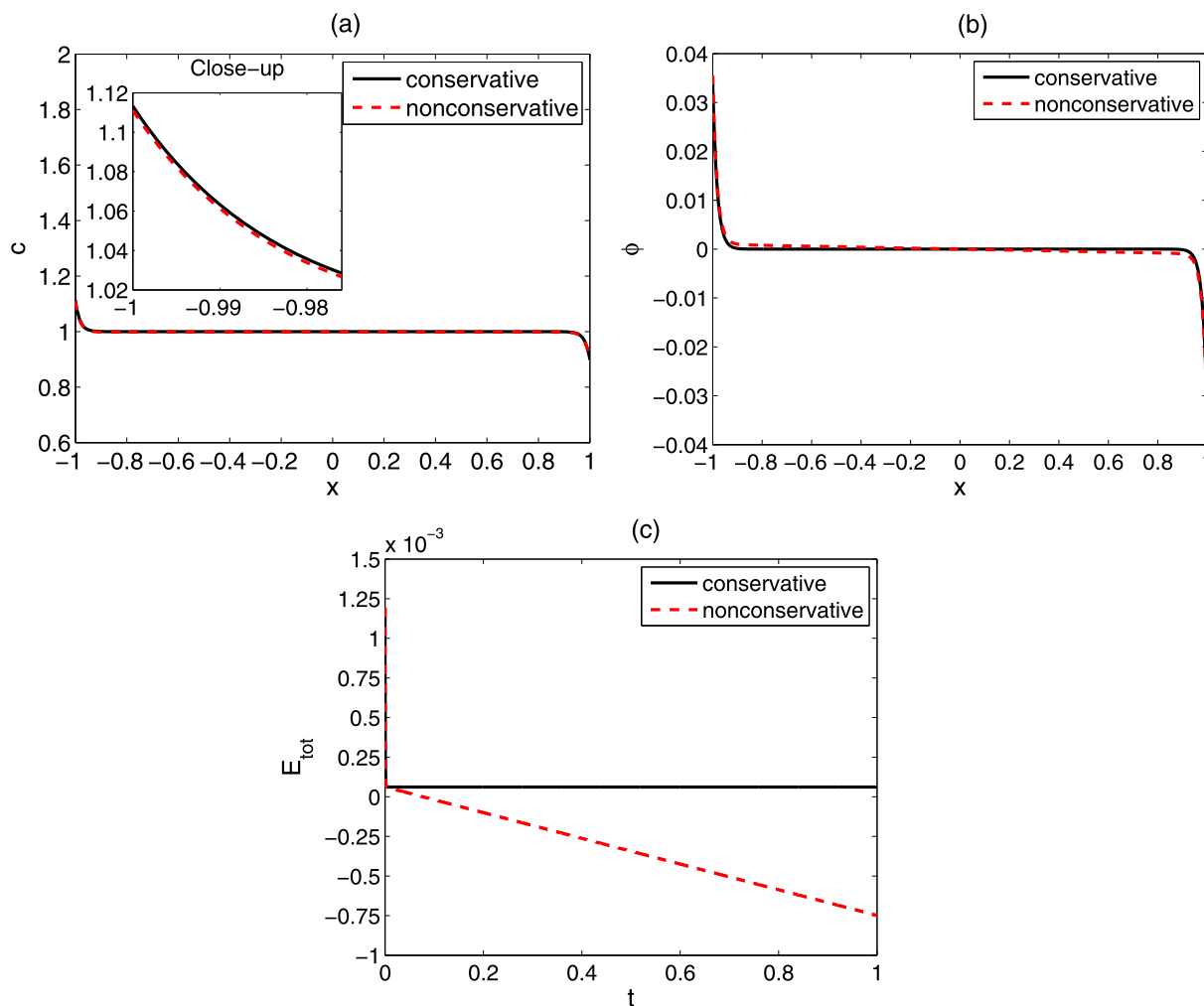
**Fig. 8** Comparison between the simulation results from the mass-conservative and the non-conservative schemes for $\eta = 0.5$. The other parameters are identical to those in Fig. 3. (**a**) The ion concentration of species 2 at the non-dimensionalized time $T = 1$. (**b**) The electric potential at the non-dimensionalized time $T = 1$. (**c**) The total energy as it varies in time

erty is shown in Fig. 8. It appears that, for $\eta = 0.5$, the total energy from the non-conservative scheme decreases linearly in time after an initial sharp drop, becoming negative at later time. On the other hand, the conservative scheme reaches a steady state very quickly and does not deviate from it. For small values of $\eta$ such as those shown in Fig. 3, both the conservation property of the total concentrations and the energy dissipation law deteriorate at a fast pace for the non-conservative scheme, and the difference between the results from the conservative and the non-conservative schemes grows bigger as $\eta$ gets smaller.

## 5 Conclusion

The primary objective of this work is to investigate the effects of conservation property of discretization schemes on the numerical results. We have shown that, with regard to

the PNP equations, whether a numerical method preserves the mass conservation could have a critical impact on the behavior of the system, especially the steady state results. We have provided a discretization scheme that preserves the mass conservation exactly (excluding the round-off errors) and the energy dissipation law well for long-time simulation.

Our method is implicit in time and second-order accurate in both space and time. We have verified that approximating the fully implicit solution is necessary for second-order convergence in time. Further, we find that one can avoid using Newton-type nonlinear solvers by performing a simple iterative scheme.

Further, we have derived the conditions on the proposed numerical scheme under which it will preserve the positivity of the concentrations.

In this work, we have simulated the equations with realistic physical parameters, particularly investigating the effect

of the non-dimensional parameters $\chi_2$ in the Poisson equation and $\eta$ in the Robin boundary condition for the electrostatic potential. We find that the mass-conserving scheme is more robust to changes in parameters, especially changes to the value of $\eta$.

Although this work makes good progress in constructing an accurate method for solving the Poisson–Nernst–Planck equations numerically, there are many challenges remaining. First, one of them is to account for the finite size of the ions as its effect is enormous considering the narrow width of the ion channels [17, 19]. Second, for most ion channels, the appropriate boundary conditions are Dirichlet-type. We will investigate the possibility to preserve the energy dissipation law exactly instead of the mass and study the effect of the conservation on long-term behavior of the simulation. Third, we would like to include distributions of permanent charges for studying selectivity of ion channels.

## References

1. Bank, R.E., Coughran, W.M. Jr., Fichtner, W., Grosse, E.H., Rose, D.J., Smith, R.K.: Transient simulation of silicon devices and circuits. IEEE Trans. Comput.-Aided Des. Integr. Circuits Syst. **CAD-4**, 436–451 (1985)
2. Bolley, C., Crouzeix, M.: Conservation de la positivité lors de la discrétisation des problèmes d'évolution paraboliques. Modél. Math. Anal. Numér. **12**(3), 237–245 (1978)
3. Cagni, E., Remondini, D., Mesirca, P., Castellani, G., Verondini, E., Bersani, F.: Effects of exogenous electromagnetic fields on a simplified ion channel model. J. Biol. Phys. **33**, 183–194 (2007)
4. Celledoni, E., Grimm, V., McLachlan, R., McLaren, D., O'Neale, D., Owren, B., Quispel, G.: Preserving energy resp. dissipation in numerical pdes using the "average vector field" method. J. Comput. Phys. **231**, 6770–6789 (2012)
5. Chiu, E., Wang, Q., Hu, R., Jameson, A.: A conservative mesh-free scheme and generalized framework for conservation laws. SIAM J. Sci. Comput. **34**, A2896–A2916 (2012)
6. Domene, C., Vemparala, S., Furini, S., Sharp, K., Klein, M.: The role of conformation in ion permeation in a k+ channel. J. Am. Chem. Soc. **130** (2008)
7. Doyle, D., Cabral, J.M., Pfuetzner, R., Kuo J. G, A., Cohen, S., Chait, B., MacKinnon, R.: The structure of the potassium channel: molecular basis of $K^+$ conduction and selectivity. Science **280** (1998)
8. Eisenberg, R.: Ion channels in biological membranes: electrostatic analysis of a natural nanotube. Contemp. Phys. **39**, 447 (1998)
9. Fisher, T., Carpenter, M., Nordström, J., Yamaleev, N., Swanson, C.: Discretely conservative finite-difference formulations for nonlinear conservation laws in split form: theory and boundary conditions. J. Comput. Phys. **234**, 353–375 (2012)
10. Gardner, C., Jones, J.: Electrodiffusion model simulation of the potassium channel. J. Theor. Biol. **291**, 10–13 (2011)
11. Gardner, C., Nonner, W., Eisenberg, R.: Electrodiffusion model simulation of ionic channels: 1d simulations. J. Comput. Electron. **3**, 25–31 (2004)
12. Gillespie, D.: Energetics of divalent selectivity in a calcium channel: the ryanodine receptor case study. Biophys. J. **94**, 1169–1984 (2008)
13. Gillespie, D., Nonner, W., Eisenberg, R.: Coupling Poisson–Nernst–Planck and density functional theory to calculate ion flux. J. Phys. Condens. Matter **14**, 12,129–12,145 (2002)
14. Ham, F., Lien, F., Strong, A.: A fully conservative second-order finite difference scheme for incompressible flow on nonuniform grids. J. Comput. Phys. **177**, 117–133 (2002)
15. Harlow, F.H., Welch, J.E.: Numerical calculation of time-dependent viscous incompressible flow of fluid with free surface. Phys. Fluids **8**, 2182 (1965)
16. Hof, B., Veldman, A.: Mass, momentum and energy conserving (mamec) discretizations on general grids for the compressible Euler and shallow water equations. J. Comput. Phys. **231**, 4723–4744 (2012)
17. Horng, T., Lin, T., Liu, C., Eisenberg, B.: PNP equations with steric effects: a model of ion flow through channels. J. Phys. Chem. B **116**, 422–441 (2012)
18. Hundsdorfer, W., Verwer, J.: Numerical Solution of Time-Dependent Advection-Diffusion-Reaction Equations. Springer Series in Computational Mathematics. Springer, Berlin (2003)
19. Hyon, Y., Eisenberg, R., Liu, C.: A mathematical model for the hard sphere repulsion in ionic solutions. Commun. Math. Sci. **9**, 459–475 (2011)
20. Kajishima, T.: Finite-difference method for convective terms using non-uniform grid. Trans. Jpn. Soc. Mech. Eng. C **65-633**(Part B), 1607–1612 (1999)
21. Lee, C., Lee, H., Hyon, Y., Lin, T., Liu, C.: New Poisson–Boltzmann type equations: one-dimensional solutions. Nonlinearity **24**, 431 (2011)
22. Li, S., Vu-Quoc, L.: Finite difference calculus invariant structure of a class of algorithms for the nonlinear Klein–Gordon equation. SIAM J. Numer. Anal. **32**, 1839–1875 (1995)
23. Lopreore, C., Bartol, T., Coggan, J., Keller, D., Sosinsky, G., Ellisman, M., Sejnowski, T.: Computational modeling of three-dimensional electrodiffusion in biological systems: application to the node of ranvier. Biophys. J. **95**, 2624–2635 (2008)
24. Markowich, P., Ringhofer, C., Schmeiser, C.: Semiconductor Equations. Springer, Berlin (1990)
25. Morinishi, Y., Lund, T., Vasilyev, O., Moin, P.: Fully conservative higher order finite difference schemes for incompressible flow. J. Comput. Phys. **143**(1), 90–124 (1998)
26. Morinishi, Y., Vasilyev, O., Ogi, T.: Fully conservative finite difference scheme in cylindrical coordinates for incompressible flow simulations. J. Comput. Phys. **197**, 686–710 (2004)
27. Nanninga, P.M.: A computational neuron model based on Poisson–Nernst–Planck theory. In: Mercer, G.N., Roberts, A.J. (eds.) Proceedings of the 14th Biennial Computational Techniques and Applications Conference, CTAC-2008, ANZIAM J, vol. 50, pp. C46–C59 (2008)
28. Neuen, C.: A multiscale approach to the Poisson–Nernst–Planck equation. Diploma Thesis, University of Bonn, Germany (2010)
29. Qiao, Z., Zhang, Z., Tang, T.: An adaptive time-stepping strategy for the molecular beam epitaxy models. SIAM J. Sci. Comput. **33**(3), 1395–1414 (2011)
30. Teorell, T.: Transport processes and electrical phenomena in ionic membranes. Prog. Biophys. Mol. Biol. **3**, 305 (1953)
31. Vasilyev, O.V.: High order finite difference schemes on non-uniform meshes with good conservation properties. J. Comput. Phys. **157**(2), 746–761 (2000)
32. Wei, G.W., Zheng, Q., Chen, Z., Xia, K.: Variational multiscale models for charge transport. SIAM Rev. **54**, 699–754 (2012)
33. Zhang, Z., Qiao, Z.: An adaptive time-stepping strategy for the Cahn–Hilliard equation. Commun. Comput. Phys. **11**(4), 1395–1414 (2012)